This is a peer-reviewed, accepted author manuscript of the following article: Shaw, A., Zhang, X., Kabalan, L., & Li, J. (2021). Mechanistic and kinetic investigation on maximizing the formation of levoglucosan from cellulose during biomass pyrolysis. *Fuel*, *286*(2), [119444]. https://doi.org/10.1016/j.fuel.2020.119444

Mechanistic and Kinetic Investigation on Maximizing the Formation of Levoglucosan from Cellulose during Biomass Pyrolysis

Alexander Shaw, Xiaolei Zhang*, Lara Kabalan, Jun Li

Department of Chemical and Process Engineering, University of Strathclyde, Glasgow, UK.

*Corresponding author: E-mail: xiaolei.zhang@strath.ac.uk, Tel: 0141 548 4131

Abstract

Attempts to understand and control the formation of levoglucosan, as a key bio-oil compound and an important intermediate chemical, during biomass pyrolysis have recently generated a large number of experimental and computational studies. Whilst promising mechanisms have been put forward to explain levoglucosan formation, there has yet to be clarity on the factors that inhibit the stoichiometric yields from cellulose, and, current available mechanisms adopt model compounds of short chain oligosaccharide structures rather than cellulose polymer. In this work, kinetic models describing cellulose (with Degree of Polymerisation DP of 2048) decomposition and levoglucosan formation have been constructed. It was found that temperature and residence time co-ordinately influenced the yield of levoglucosan, i.e. maximum yield can be reached within 80 seconds at 600 ^{o}C, however, around 10 minutes is required at 550 ^{o}C. Anhydro-oligosaccharides greater than DP8 will be generated and then consumed in 60 seconds with pyrolysis temperatures of 500 ^{o}C and over. The results

also showed that the current available concerted initiation and depropagation reactions are insufficient to explain the experimentally observed high rates of cellulose depolymerisation and levoglucosan formation, other key factors such as side reactions have to be considered. Additionally, it was found that the rate of levoglucosan generation is independent of the initial cellulose chain length, which is a finding that will facilitate future studies in the area of bioenergy and biomass decomposition.

Keywords: Levoglucosan; Cellulose; Concerted reaction; Density functional theory; Reaction rate

1. Introduction

Biomass is a renewable energy resource that can be derived from agricultural and forestry sources, including by-products of the timber industry, agricultural crops, and animal manures. An additional source includes a considerable proportion of municipal solid waste. The high natural abundance and potential for carbon neutrality that biomass utilization affords makes it both environmentally and economically important [1–5]. It has been reported that bioenergy provided about 5% of total primary energy use in the United States in 2018 [6]. Of that 5%, about 51% was from solid biofuels, 41% was from liquid fuels, and the remainder was from biogases and municipal waste. As of 2019, 11 % of UK's electricity is provided from biomass as described by the Renewable Energy Association (REA) [7]. According to the same REA report, bioenergy provides 96% of non-domestic renewable heat (including biomass boilers and biomethane) and contributes 7.4% of the country's total energy needs.

Levoglucosan (LG), one of the primary products of biomass pyrolysis [8–10], has attracted significant research interest due, in part, to its potential use in the production of monomeric sugars which can subsequently be utilized to produce biofuels such as ethanol and butanol. Other potential uses of LG include the manufacturing of biodegradable polymers,

surfactants, and pharmaceuticals compounds, amongst other products [11]. Much effort has been dedicated to understand the mechanisms for LG formation during biomass pyrolysis, or essentially cellulose pyrolysis. In the reaction models of Broido et al. [12,13] and Shafizadeh et al. [14], cellulose pyrolysis is considered as a sequence of multistep reactions wherein cellulose will first decompose to form a reactive intermediate that they named 'active cellulose'. This active intermediate may then decompose to form volatiles and char. The work of Lédé et al. [15] showed that 'active cellulose' consists of a transient liquid compound composed primarily of short chain anhydro-oligosaccharides, including small amounts of LG and cellobiosan.

Whilst LG is one key product from cellulose pyrolysis, its yield varies significantly with different operating conditions including temperature, heating rates and reactor type. Shen and Gu [16] obtained 62.2% LG in quartz tube reactor at a temperature of 530 ^{o}C. Increasing the residence time reduced this yield to 53.1%, whilst increasing the reaction temperature to 630 ^{o}C at the shorter residence time reduced the yield to 51.1%. Patwardhan et al. [17] achieved yields of 58.8% at 500 ^{o}C using a single shot micropyrolyser whilst Lindstrom et al. [18] reported LG yields of 54.4% using a CPD-Quench micropyrolyser at the same temperature. Kwon et al. [19] reported LG yields as high as 70% from lab-scale pyrolysis at reduced pressure, but as low as 20% from laser-induced cellulose pyrolysis within a nitrogen environment [20], which was blamed on the generation of an inhibiting aerosol caused by the small heating are of the laser that allowed for product condensation. Dobele et al. [21] also reported a low yield of 20.4% LG from the pyrolysis of cellulose on a microgram-scale although the reason for this relatively small yield is unclear. The wide ranging yields suggests that temperature and reaction conditions play a critical role in controlling the rate of formation of LG and the competition between LG forming reactions and the generation of alternative cellulose pyrolysis products.

Computational modelling studies have also played a key role in elucidating the formation mechanisms of LG from cellulose. Our previous work [22,23] investigated the homolytic cleavage of cellobiose into two glucosyl radicals, as well as the heterolytic fission routes to produce two pairs of corresponding ionic monosaccharides. The significant barrier heights for the heterolytic routes ruled them out as primary pathways for the cleavage of cellobiose, whilst the homolytic cleavage pathways were more reasonable. Following dissociation of the glycosidic bonds at either end of a cellulose monomer, a glucopyranose biradical can then undergo rearrangements and C-O bond formation to yield LG. Mayes and Broadbelt [24] reported a concerted method for the simultaneous depolymerisation of cellulose and formation of LG. In the first step, termed 'concerted initiation', this 'chain-end' mechanism liberates a glucose molecule from the reducing end (RE) of a cellulose chain and produces an LG chain-end. A subsequent 'concerted depropagation' reaction will liberate this LG molecule and produce another LG chain-end, which will, in-turn, be cleaved from the cellulose polymer. When considering the non-reducing end (NRE) of the cellulose, the initiation and depropagation reactions become a single step LG forming reaction. A comparison study performed in our previous work [25] confirmed that the concerted mechanism is more facile than either the hydrolytic-glucose intermediate route or the homolytic pathway and agreed closely to experimental measurements of the energetics of LG formation.

Vinu and Broadbelt [26] considered four variants of the concerted reaction in their mechanistic model of carbohydrate pyrolysis. These consisted of a mid-chain initiation, the aforementioned depropagation, an NRE initiation, and the end chain concerted initiation. The authors also propose that hydrolysis plays a dominant role in cellulose depolymerisation and that considerable yields of glucose should be formed as a result, however, glucose has not been identified as a major intermediate during cellulose pyrolysis [27,28]. Furthermore, the water is posited to be derived through cellulose dehydration reactions, however, the calculated reaction

barriers for cellulose dehydration range from 63.2 – 99.1 kcal mol^{-1} and appear too high for the generation of water in significant quantities [29]. For a single cellulose chain, one instance of the concerted initiation will convert a glucose chain-end into an LG chain-end, from which no more concerted initiations may take place. No other proposed reactions lead to the reformation of a glucose chain-end and so the role of the concerted initiation in cellulose conversion must be minimal. Discarding this reaction allows for the depolymerisation of cellulose to be considered as a competition of the three remaining reactions. A mid-chain initiation will split a cellulose polymer into two separate chains, producing an LG-type RE and also an NRE. Each type of chain-end can then undergo its respective depropagation reaction to produce a molecule of LG and an equivalent chain-end.

The previously proposed mechanisms for LG formation are generally limited to dimers and trimers of cellulose and anhydrocellulose, however the experimental works of Lindstrom et al. [18] and of Proano-Aviles [30] show clearly that the generation of LG is dictated by a balance of mid-chain cracking and chain-end LG generating reactions, highlighting the importance of considering cellulose polymers rather than short chain oligosaccharide structures. Additional kinetic investigation on depolymerisation and LG formation from cellulose polymer is yet to be reported. Such information is clearly necessary for advancement of LG formation technologies. In this paper we will firstly investigate the cellulose polymer degradation pathways, beginning from a cellulose chain with a DP of 2048, which will be done by exploring the kinetics of cellulose mid-chain depolymerisation reactions, chain-end LG formation reactions, and LG ring-opening and dehydration mechanisms. Secondly, based on the obtained cellulose degradation pathways, the optimum operating conditions (e.g. temperature. Reaction time, cellulose chain length) to maximise the LG yield will be explored.

2. Methodology

Density functional theory (DFT) calculations were employed to calculate the geometries and energies of all pathways in this study. The M06-2X functional [31] was used in conjunction with the def2-TZVP [32] basis set in all reactions considered in the kinetic model. The D3 dispersion correction [33] with zero damping factor was used throughout. All ground state structures were confirmed to have zero imaginary frequencies and all transition states were confirmed to have exactly one imaginary frequency. The correctness of all transition state structures were confirmed through visual assessment of the imaginary frequency mode and intrinsic reaction coordinates analysis. Gaussian 16, Rev C.01 [34] was used for all calculations with an integration grid size of 99,590 points.

The Eyring equation (Equation 1) was used to derive the temperature dependent rate constant for each elementary reaction using the Gibb's free energy of activation obtained from the DFT calculations at temperatures in 50 ºC increments from 400 ºC to 800 ºC.

$$k = \frac{k_B T}{h} e^{-\Delta G^*/(RT)} \qquad \text{Equation 1}$$

where ΔG* is the Gibbs free energy of activation, k_B is the Boltzmann constant ($1.381E10^{-23}$ J K^{-1}), T is the temperature (K), h is the Planck constant ($6.626E10^{-34}$ J·s) and R is the gas constant (8.314 J K^{-1} mol^{-1}). This data was supplied to an in-house kinetic model in order to calculate the time dependent concentrations of species of interest using an ordinary differential equation (ODE). An ODE of order n is an equation of the form: $F(x, y, y', \ldots, y^n) = 0$ where here y is a function of x, $y' = dy/dx$ is the first derivative with respect to x and $y^n = d^n y/dx^n$ is the n derivative with respect to x. A simple example if A → B with a rate constant k, considering the reaction is irreversible dA/dt would be equal to $-k[C_A]$, where C_A is the concentration of A, and $dB/dt = -k[C_B]$, where C_B is the concentration of B. At t = 0 we have considered that the concentration of A is equal to 1 and the concentration of B is equal 0. This equation has been applied to all the pathways using the rate constant of each of the steps.

144 A cellulose chain with DP of 2048 was chosen as the starting point, which is a reasonably close
145 to the DP value of 1871 for cellulose reported by Lindstrom et al. [18].

146 **3. Results and Discussion**

147 *3.1* Overview of the reactions considered in this work

148 The main reactions involved in the process of converting cellulose to levoglucosan will
149 be investigated in this section, this will serve as the foundation to the following sections on
150 exploring the products (e.g. anhydro-oligosaccharides, cellotriosan, cellobiosan, LG) yields.
151 The reactions include four concerted cellulose depolymerisation reactions and six LG
152 decomposition reactions. The Gibbs free energy of activation and the rate constant for each
153 reaction were calculated at a temperature range of 400-800˚C in this work, which are lacking
154 information in the literature.

155 *3.1.1 Four concerted cellulose depolymerisation reactions*

156 The four concerted depolymerisation reactions involved in the cellulose decomposition
157 process are outlined in Figure 1. The Gibbs free energy of activation and rate constants for
158 these four reactions under temperatures of 400-800 ^{o}C are shown in Table 1.

Figure 1. The four concerted depolymerisation reactions from cellulose polymer considered in this work.

The mid-chain initiation reaction involves the cleavage of the central glycosidic linkage of cellotetraose to generate cellobiosan and cellobiose, representing the newly generated LG-type RE and glucose-type NRE, respectively. This reaction provides the kinetic values for all non-chain-end cleavage reactions of celluloses larger than DP = 3. A validation study regarding the selection of cellotetraose is provided in section S1 of the supplementary information. The Gibbs free energy of activation for the mid-chain initiation reaction at 25 ^{o}C is 50.4 kcal mol^{-1} [1]. As the temperature increases, a small rise in the activation free energy (as shown in Table 1) for mid-chain initiation is observed, meaning that the increasing of rate constants at higher temperatures are slightly diminished.

Table 1. Gibbs free energy of activation and rate constants for the four concerted depolymerisation reactions at 50 ^{o}C increments from 400 ^{o}C to 800 ^{o}C.

	Mid-chain initiation		RE-depropagation		NRE-depropagation		Cellobiosan cleavage	
Temperature (°C)	ΔG_{act}^{*}	Rate Constant†	ΔG_{act}^{*}	Rate Constant†	ΔG_{act}^{*}	Rate Constant†	ΔG_{act}^{*}	Rate Constant†
400	52.1	$1.73E10^{-4}$	55.9	$1.03E10^{-5}$	53.8	$4.96E10^{-5}$	57.7	$2.59E10^{-6}$
450	52.3	$2.42E10^{-3}$	55.9	$1.90E10^{-4}$	53.8	$8.50E10^{-4}$	57.7	$5.50E10^{-5}$
500	52.4	$2.41E10^{-2}$	56.0	$2.40E10^{-3}$	53.8	$1.01E10^{-2}$	57.7	$7.89E10^{-4}$
550	52.6	$1.81E10^{-1}$	56.1	$2.24E10^{-2}$	53.8	$8.90E10^{-2}$	57.8	$7.74E10^{-3}$
600	52.8	$1.09E10^{0}$	56.1	$1.62E10^{-1}$	53.8	$6.11E10^{-1}$	57.8	$6.21E10^{-2}$
650	53.0	$5.35E10^{0}$	56.2	$9.73E10^{-1}$	53.9	$3.41E10^{0}$	57.8	$3.99E10^{-1}$
700	53.2	$2.24E10^{1}$	56.3	$4.60E10^{0}$	53.9	$1.60E10^{1}$	57.8	$2.12E10^{0}$
750	53.5	$8.16E10^{1}$	56.4	$1.92E10^{1}$	53.9	$6.43E10^{1}$	57.9	$9.15E10^{0}$
800	53.7	$2.64E10^{2}$	56.5	$7.04E10^{1}$	54.0	$2.28E10^{2}$	57.9	$3.62E10^{1}$

*The unit for Gibbs free energy of activation, ΔG_{act}, is kcal/mol. †The unit for all rate constants is s^{-1}.

The RE-depropagation consists of the cleavage of the RE glycosidic linkage of cellotriosan to yield cellobiosan and LG, and is representative of all RE-chain end cleavage reactions. For the RE-depropagation, cellotriosan is selected as the model compound. The RE-depropagation reaction has a free energy of activation of 55.5 kcal mol^{-1} at 25 °C, which is notably larger than the mid-chain initiation reaction, highlighting the importance of obtaining separate kinetic data for chain-end and mid-chain reactions. The temperature dependant rate constants for this reaction, given in Table 1, are over a factor of 10 lower than for the mid-chain cleavage at 400 °C and close to a factor of 4 slower at 800 °C. It is clear from this that mid-chain initiation reactions will occur at significantly more frequently than RE-depropagation reactions, particularly when considering the vastly greater number of mid-chain bonds compared to chain-ends in the early stages of the reaction.

The NRE-depropagation reaction involves cleavage of the RE linkage to yield LG and cellobiose, representing the generated NRE environment. Cellotriose was chosen over

cellotriosan due to the presence of the anhydro-glucose residue in the latter which, for any anhydrosugar with a DP greater than 3, would not be in close proximity to the cleaved linkage. The Gibbs free energy barrier height for this reaction is 53.8 kcal mol^{-1} which is 1.7 kcal mol^{-1} lower than the RE-depropagation at the same temperature, 25 ^{o}C, suggesting that NRE-depropagation may be the dominant LG forming reaction. Whilst the difference in free energy barriers for the two depropagation reactions is relatively small, it adds further support to the notion that each cleavage reaction must be considered separately. The rate data given in Table 1 shows that the NRE-depropagation is almost a factor of 5 faster than the RE-depropagation at 400 ^{o}C. Whilst this is reduced to a factor of 3 at 800 ^{o}C, the NRE-depropagation is still the dominant LG forming reaction at higher temperatures.

The cleavage of cellobiosan to form two LG is also modelled explicitly as neither of the depropagation reactions would accurately represent the cellobiosan environment. The structures of all reactants, transition states and products are provided in section S2 of the supplementary information. From the temperature dependant values given in Table 1, we observe that the Gibbs free energy of activation for cellobiosan cleavage is around 4.0 kcal mol^{-1} higher than for NRE-depropagation and at least 1.5 kcal mol^{-1} larger than RE-depropagation. Accordingly, the rate constants for LG formation from cellobiosan are slower than for LG formation from either chain-end reaction. Clearly, any kinetic model that assumes that the rate constants for the cleavage of cellobiosan are equivalent to all cellulose cleavage reactions will obtain a much slower rate of LG formation than predicted by the present kinetic data.

The free energy barriers for the initiation and depropagation reactions given in Table 1 agree very well with the results from Mayes and Broadbelt [24], who obtained a free energy barrier height of 54.4 kcal mol^{-1} for the cleavage of methyl-cellobiose and 56.6 kcal mol^{-1} for the splitting of methyl-cellobiosan, both at 500^{o}C. Our early comparison study [25] observed

lower free energy barriers of 46.1 kcal mol^{-1} and 43.7 kcal mol^{-1}, for cellobiose cleavage and cellobiosan cleavage, respectively. Zhang et al. [35] also obtained a low barrier for cellobiose cleavage, reporting an enthalpy of activation of 48.4 kcal mol^{-1}. These lower energy barriers suggested that additional glucosyl units have a significant impact on the bond cleavage energy requirements.

3.1.2 Levoglucosan decomposition reactions

The degradation of LG via numerous reaction pathways has been reported previously [36,37], however, only the more facile reactions are considered in this work. Typically, LG ring opening is proposed to occur via three mechanisms [36,37], two involving C-O bond fission and one C-C bond breaking pathway. Two of these reactions are predicted to have energy barriers sufficiently large as to render their influence on the degradation of LG negligible at moderate pyrolysis temperatures. The C-O breaking reaction shown in Figure 2 is predicted to be several orders of magnitude quicker than the alternative ring opening reactions and is therefore the only one considered in this study. Following the ring opening step, one of two retro-aldol reactions, shown in Figure 2, will occur rapidly, inhibiting the reformation of LG from the open ring species.

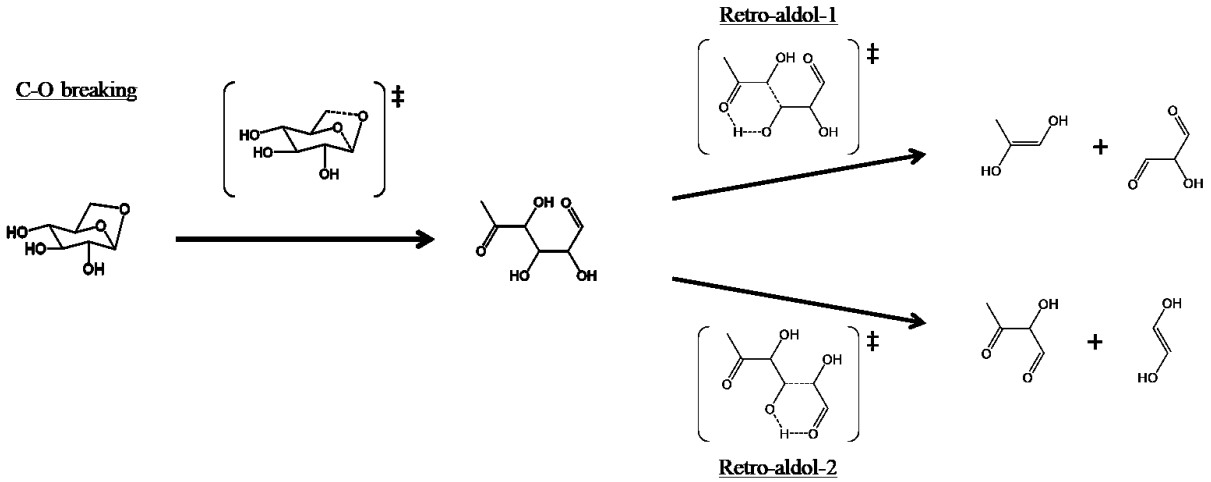

228 Figure 2. LG ring opening through C-O breaking and two subsequent retro-aldol reactions
229 used in the kinetic model.

230 There are six potential mechanisms for the dehydration of LG, four of which are
231 included in this work as shown in Figure 3. The two excluded pathways have been shown to
232 exhibit significantly higher energy barriers [36,37] due to the generation of a double bond
233 involving one of the bridgehead carbons, thus inducing significant strain within the system.

234

235 Figure 3. Four dehydration reactions of LG included in the kinetic model.

236 The Gibbs free energy of activation for the LG C-O breaking reaction at 25 ^{o}C is 69.4
237 kcal mol^{-1} and the temperature dependent rate constants are given in Table 2. The Gibbs free
238 energy of the ring-opening is largely independent of the reaction temperature. The free energy
239 of activation for retro-aldol 1 at 25 ^{o}C is 34.4 kcal mol^{-1} and for the retro-aldol 2 it is 36.7 kcal
240 mol^{-1}. The temperature dependent rate constants of both reactions are given in Table 2. The
241 relatively low reaction barrier heights for both retro-aldol reactions leads to large rate constants
242 and a rapid consumption of the open-ring intermediate compound. In our earlier work [36], we
243 calculated the enthalpy barrier for LG C-O breaking to be 62.9 kcal mol^{-1}, at the same level to
244 the value in the current work. A recent work from Guo et al. [37] gave a barrier height for this

reaction of just 54 kcal mol^{-1}, however, considerable differences in their computational approach are likely account for this significant variation.

Table 2. Gibbs free energy of activation and rate constant for LG C-O breaking and two retro-aldol reactions at 50 °C increments from 400 °C to 800 °C.

	LG C-O breaking		Retro-aldol 1		Retro-aldol 2	
Temperature (°C)	ΔG_{act}*	Rate Constant†	ΔG_{act}*	Rate Constant†	ΔG_{act}*	Rate Constant†
400	69.4	$4.13E10^{-10}$	35.7	$3.60E10^{1}$	36.7	$1.71E10^{1}$
450	69.4	$1.60E10^{-8}$	35.9	$2.13E10^{2}$	36.9	$1.06E10^{2}$
500	69.4	$3.89E10^{-7}$	36.1	$1.01E10^{3}$	37.1	$5.25E10^{2}$
550	69.4	$6.44E10^{-6}$	36.4	$3.72E10^{3}$	37.3	$2.14E10^{3}$
600	69.5	$7.32E10^{-5}$	36.6	$1.26E10^{4}$	37.5	$7.48E10^{3}$
650	69.5	$6.77E10^{-4}$	36.8	$3.73E10^{4}$	37.7	$2.29E10^{4}$
700	69.5	$5.00E10^{-3}$	37.0	$9.95E10^{4}$	37.9	$6.25E10^{4}$
750	69.5	$3.04E10^{-2}$	37.2	$2.41E10^{5}$	38.2	$1.48E10^{5}$
800	69.6	$1.57E10^{-1}$	37.5	$5.16E10^{5}$	38.4	$3.38E10^{5}$

*The unit for Gibbs free energy of activation, ΔG_{act}, is kcal/mol. †The unit for all rate constants is s^{-1}.

The Gibbs free energy of activation for the dehydration reactions at 25 °C range from 65.7 kcal mol^{-1} for dehydration 3 to 71.8 kcal mol^{-1} for dehydration 2 at 25 °C and the temperature dependent rate constants for all four reactions are given in Table 3. It shows that the LG dehydration 3 is the most energetic preferred dehydration pathway and its energy barrier is lower than the C-O breaking step as shown in Table 2. These results agree well with previous

256 ranges in energy barriers for these four dehydration reactions of 63.6 – 68.6 kcal mol^{-1} in our
257 earlier study [36] and 62 – 65 kcal mol^{-1} for Guo et al. [37].

258 *Table 3. Gibbs free energy of activation and rate constant for the four LG dehydration*
259 *reactions at 50 °C increments from 400 °C to 800 °C.*

	LG dehydration 1		LG dehydration 2		LG dehydration 3		LG dehydration 4	
Temperature (°C)	ΔG_{act}^{*}	Rate Constant†	ΔG_{act}^{*}	Rate Constant†	ΔG_{act}^{*}	Rate Constant†	ΔG_{act}^{*}	Rate Constant†
400	69.4	$4.13E10^{-10}$	71.6	$7.97E10^{-11}$	65.9	$5.65E10^{-9}$	67.8	$1.36E10^{-9}$
450	69.4	$1.60E10^{-8}$	71.6	$3.46E10^{-9}$	65.9	$1.83E10^{-7}$	67.8	$4.88E10^{-8}$
500	69.4	$3.89E10^{-7}$	71.5	$9.91E10^{-8}$	65.9	$3.79E10^{-6}$	67.8	$1.10E10^{-6}$
550	69.4	$6.44E10^{-6}$	71.5	$1.78E10^{-6}$	65.9	$5.47E10^{-5}$	67.8	$1.71E10^{-5}$
600	69.5	$7.32E10^{-5}$	71.5	$2.31E10^{-5}$	65.9	$5.83E10^{-4}$	67.9	$1.84E10^{-4}$
650	69.5	$6.77E10^{-4}$	71.4	$2.40E10^{-4}$	66.0	$4.56E10^{-3}$	67.9	$1.62E10^{-3}$
700	69.5	$5.00E10^{-3}$	71.4	$1.87E10^{-3}$	66.0	$3.06E10^{-2}$	67.9	$1.14E10^{-2}$
750	69.5	$3.04E10^{-2}$	71.3	$1.26E10^{-2}$	66.0	$1.70E10^{-1}$	67.9	$6.69E10^{-2}$
800	69.6	$1.57E10^{-1}$	71.3	$6.75E10^{-2}$	66.0	$8.10E10^{-1}$	67.9	$3.32E10^{-1}$

*The unit for Gibbs free energy of activation, ΔG_{act}, is kcal/mol. †The unit for all rate constants is s^{-1}.

260

261 *3.2* Cellulose Depolymerisation

262 *3.2.1 General description of the cellulose depolymerisation process*

263 Due to the significantly greater number of sites in a DP = 2048 cellulose for mid-chain
264 initiation over the chain-end depropagation reactions, mid-chain depolymerisation is the
265 dominant reaction in the early stages of cellulose pyrolysis. Owing to this, and in order to
266 further simplify the kinetic model, mid-chain initiation is the only reaction that is considered
267 until the average DP of the cellulose is reduced to 16, after which all concerted reactions are
268 considered in parallel. An abbreviated form of the reaction network is shown in Figure 4.

A DP = 16 anhydrocellulose can undergo one of the two chain-end reactions, an NRE-depropagation or an RE-depropagation, both of which give rise to LG and a DP = 15 anhydrocellulose. Alternatively, there are 13 glycosidic linkages which may participate in mid-chain initiation reactions. Each of these reactions produces two further anhydrocellulose fragments and are all considered kinetically equivalent. The resulting anhydrocellulose fragments can all engage in further chain-end and mid-chain cleavages while DP > 3. Cellotriosan (DP = 3) is unable to undergo mid-chain cleavage but may produce LG and cellobiosan (DP = 2) through either an RE-depropagation or an NRE-depropagation. Cellobiosan will yield 2 molecules of LG as shown in Figure 1. LG will then undergo a ring opening/retro-aldol reaction pathway or proceed through one of four dehydration reactions. In either case, the products are termed ‘Degradation Products’ and consideration of any further reactions is unnecessary.

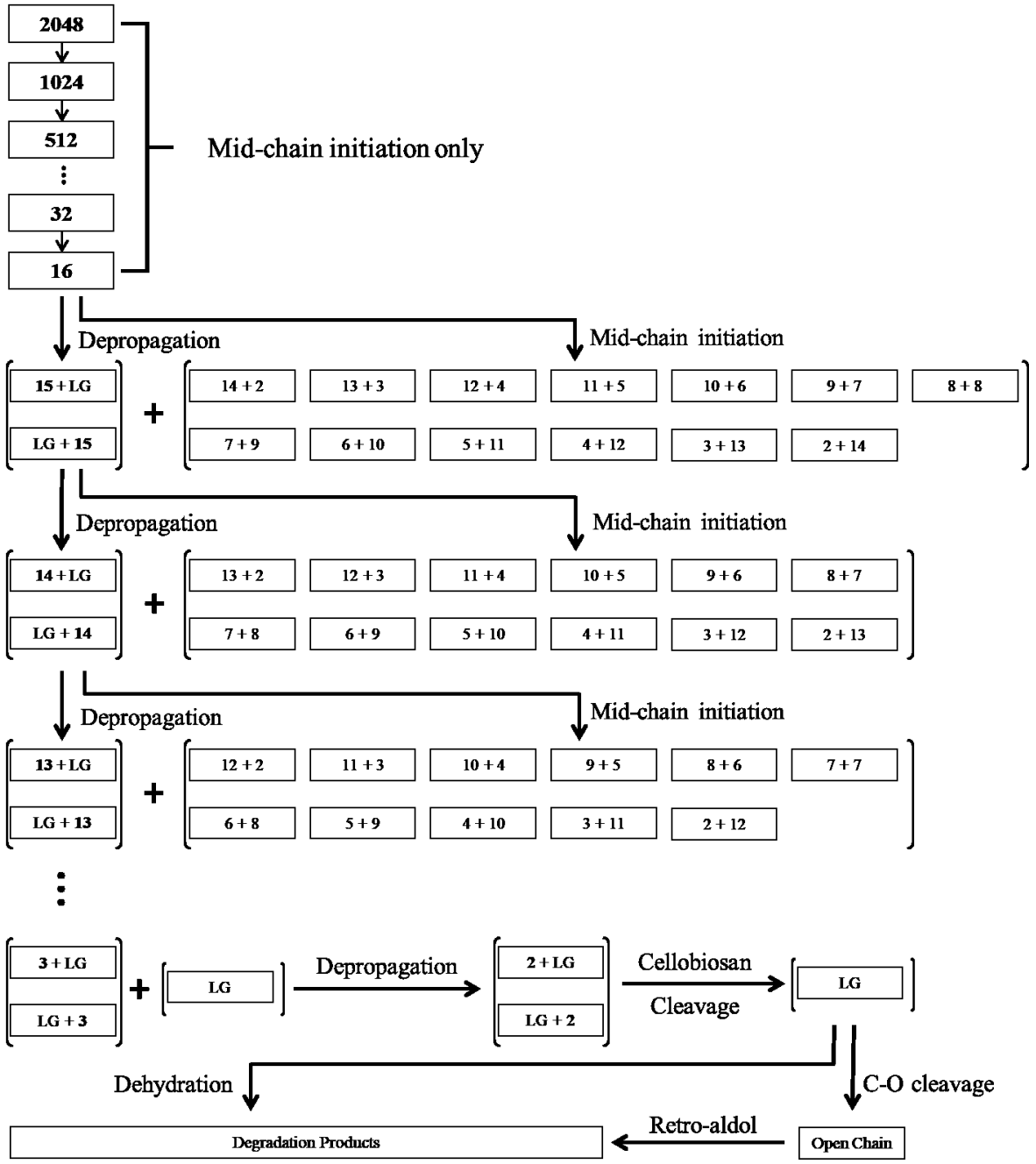

Figure 4. Reaction network from which the kinetic model is constructed. The reactions involving DP = 256-64 and DP = 12-4 are not shown but are included explicitly in the kinetic model.

3.2.2 Molar amounts and mass profiles of anhydrocellulose depolymerisation from DP = 2048 to LG

Figure 5 shows both the molar amounts (decomposing from 1mol of cellulose DP = 2048) and masses (decomposing from 332.06 kg of cellulose DP = 2048) of select anhydrocellulose chains, with a DP ranging from 2048 down to 1 (LG) at 500 ºC, 550 ºC and 600ºC. These temperatures were selected as the key range based upon the rate constant calculations.

[redacted]

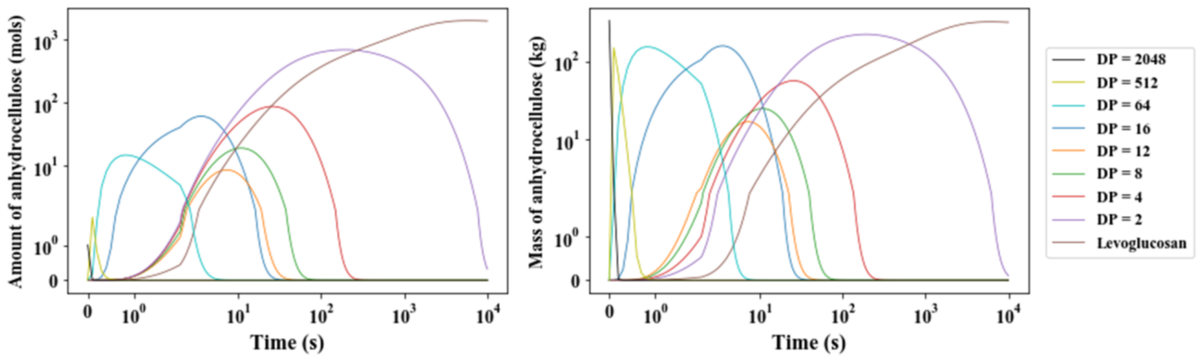

[redacted]

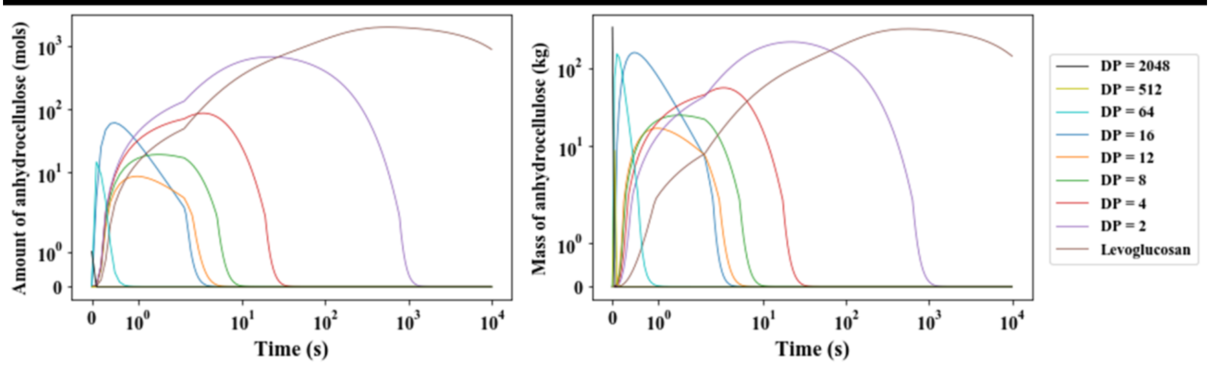

[redacted]

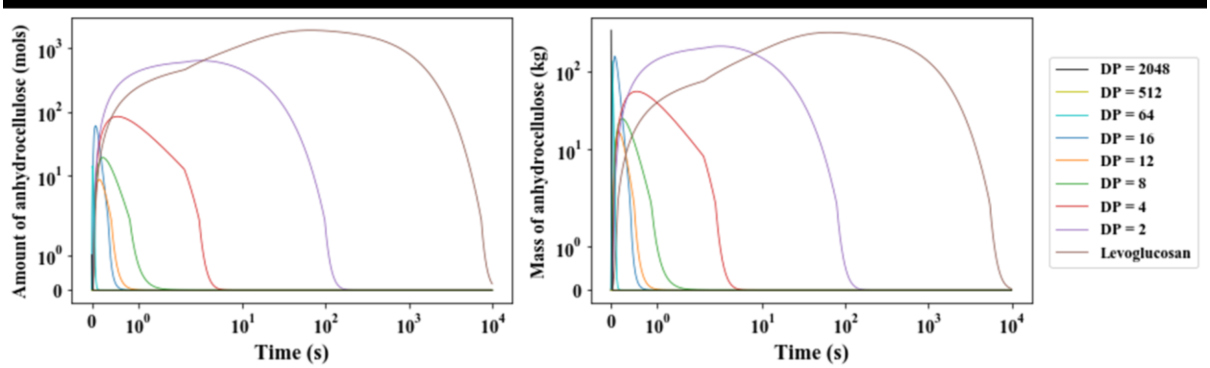

Figure 5. Time dependent changes in the relative molar amounts and masses of anhydrocelluloses with lengths from 2048 to 1.

At 500 °C, the degradation of the starting polymer is completed almost instantaneously, as is the conversion of the DP = 512 intermediate. Chains with DPs in the range of 512 – 64 will disappear within the first 10 seconds of pyrolysis whilst DP = 16-8 chains require between 50-100 seconds to be converted. Cellotetraosan (DP=4) and cellobiosan DP=2 take considerable longer to be converted, requiring around 400 and 10,000 seconds, respectively. Accordingly, the maximum amount of LG is not realised until around 10,000 seconds also. At 550 °C, chains as short as DP = 8 are consumed within the first 10 seconds, around a factor of ten faster than at 500 °C. Even cellotetraosan masses reach zero after around 50 seconds. The complete conversion of cellobiosan and the point of maximum LG yield are still not reached until around 1000 seconds, far longer than would be expected of typical pyrolysis regimes. At 600 °C, anhydrocellulose chains greater than DP = 12 are lost in under 1 second and even cellotetraosan should be entirely converted well within the first ten seconds. The complete consumption of cellobiosan and the maximum formation of LG require over 100 seconds, even at this elevated temperature.

3.3 Levoglucosan formation

3.3.1 Influence of temperature and reaction time

The rapidly depolymerising cellulose leads to the generation of large numbers of chain-ends as active sites, these active sites are precursors for the generation of LG. For the initial cellulose chain, the number of active sites is 2. As shown in Figure 6, the relative number of active sites reaches a maximum within a few seconds at 600 °C, before diminishing as LG is formed. This reduction in active sites would correlate to a disappearance of the ‘active cellulose’ intermediate. The maximum number of active sites appears around 10 seconds at

550 ºC and the conversion to LG occurs over 600 seconds. At 500 ºC, the process is significantly slower and a large number of unconverted chain-ends are still present after 600 seconds.

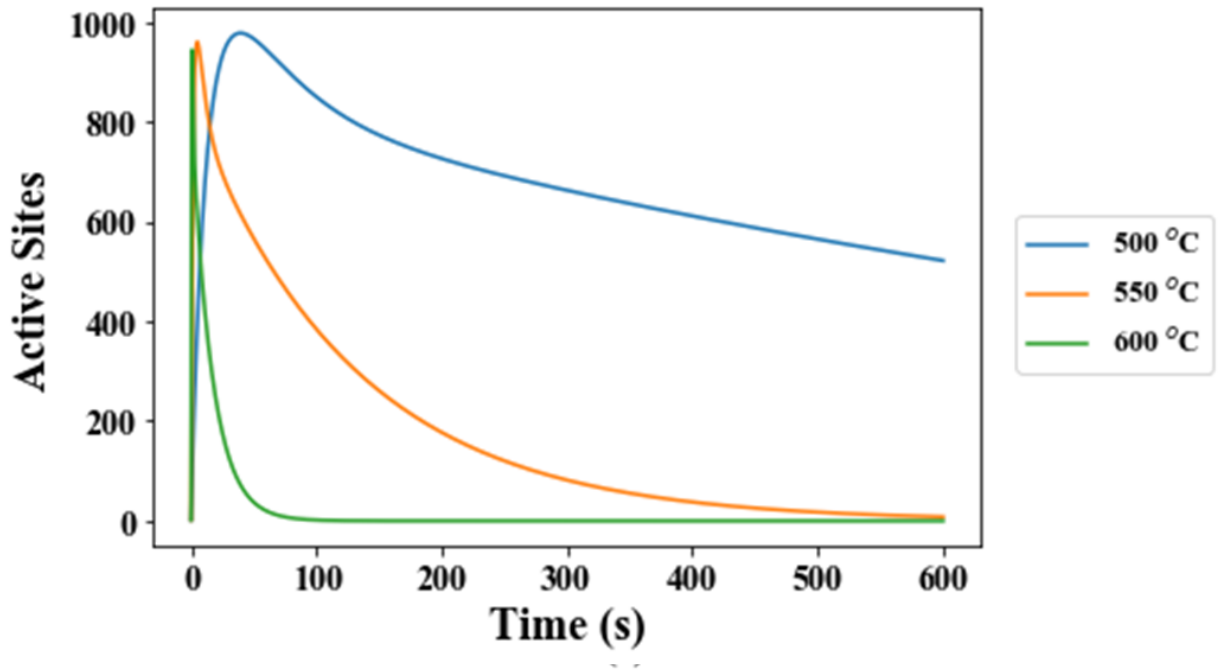

Figure 6 Time dependent changes in the number of active-sites present relative to the initial cellulose polymer over 600 seconds.

Figure 7 gives the relative yields of LG over time, as well as the theoretical maximum LG yield. The values for 650 ºC have been included to highlight more clearly the effect of temperature on LG degradation. At 600 ºC and 650 ºC, a maximum LG yield is reached very rapidly, whilst at 550 ºC, around 10 minutes are needed to reach maximum yield. At 500 ºC, the formation rate of LG is considerably slower, requiring much longer than typical pyrolysis times.

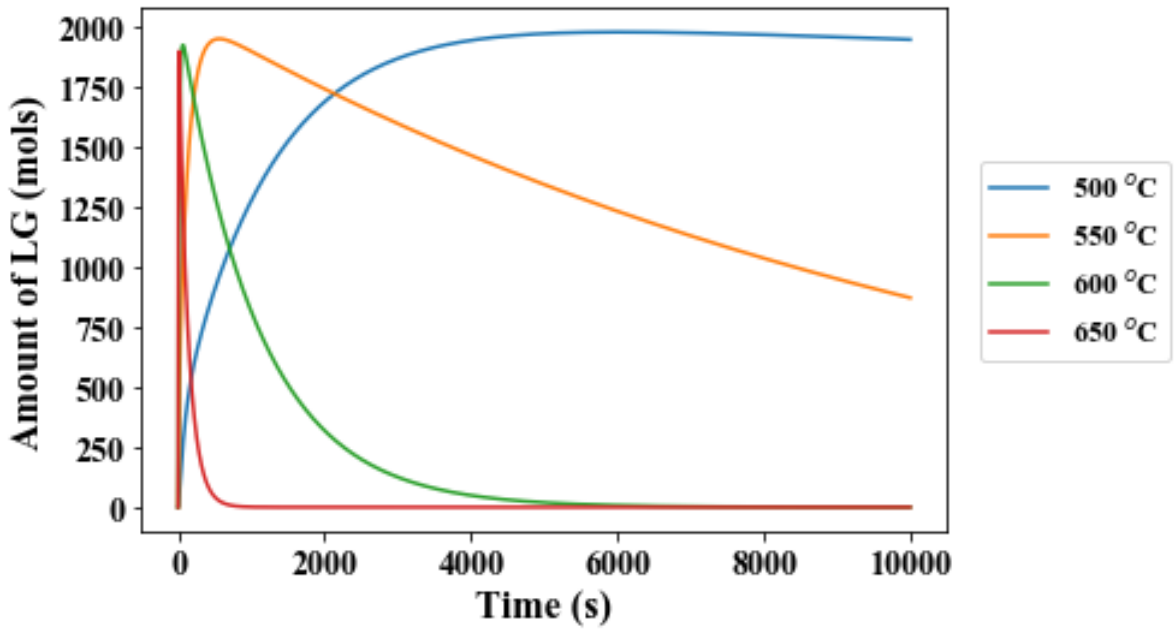

Figure 7. Time dependent changes in the molar amount of levoglucosan over 10000 seconds.

3.3.2 Influence of cellulose chain length

One important observation from the kinetic modelling is that the yield of LG over time is largely unaffected by the initial anhydrocellulose chain length. As shown in Figure 8, the time required to reach maximum LG yield at 600 ºC is the same for all four initial chain lengths. The crossing point of the 550 ºC and 600 ºC are also identical for all four starting chain lengths, as is the final LG mass after 300 seconds at 500 ºC, showing that it is not a temperature specific phenomenon.

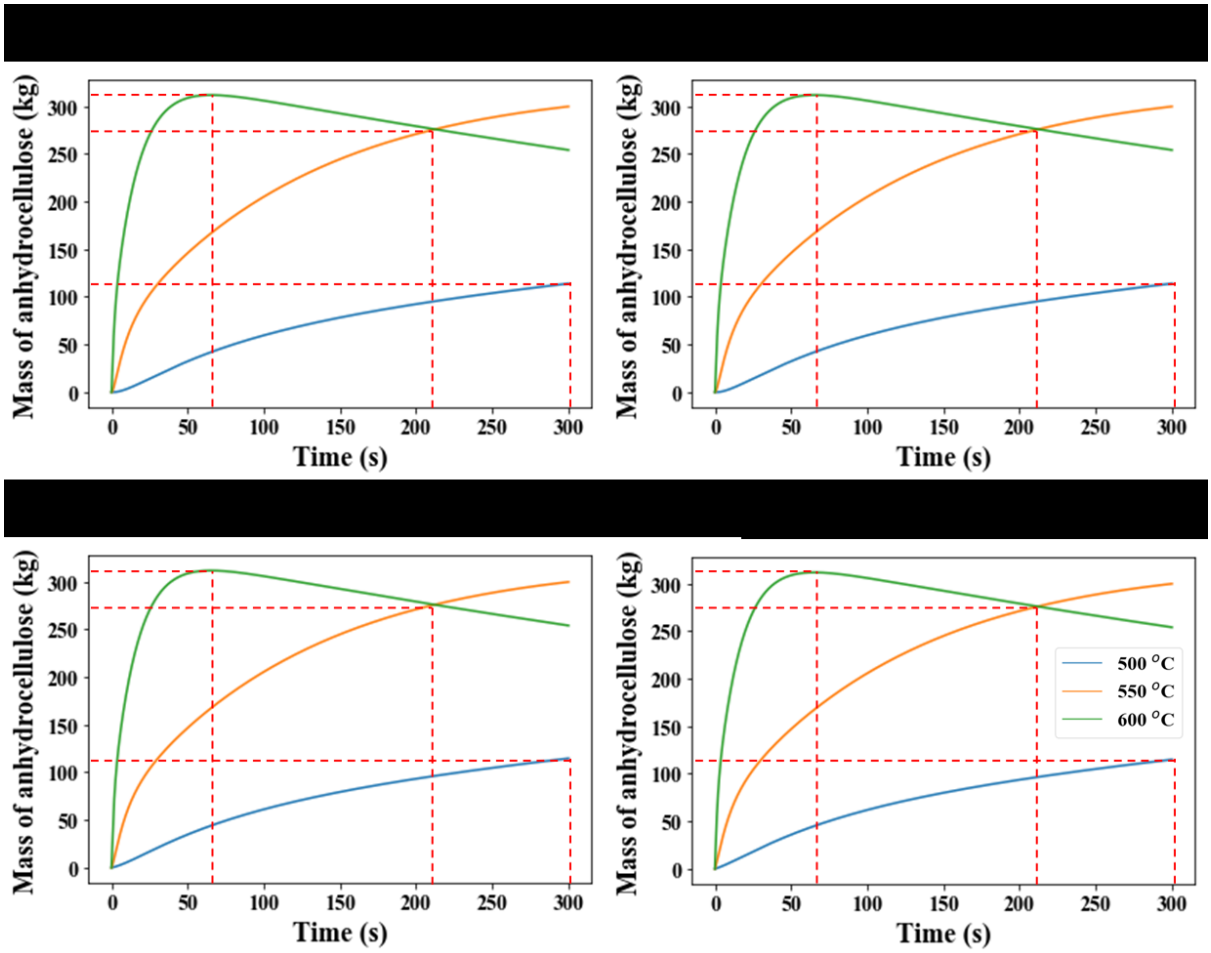

Figure 8. Levoglucosan yields from anhydrocelluloses of initial DPs = 2048, 512, 12 and 8.

One key benefit of this finding is the potential simplification of cellulose pyrolysis models, where inclusion of polymer lengths is not required, leading to a considerable reduction in the number of explicitly included reactions taking place. This should also mean that the maximum detectable oligo-saccharides at each pyrolysis temperature should also be unrelated to the initial polymer length, with the obvious caveat that the initial length is larger than the expected maximum DP. Whether these assumptions hold true under experimental conditions, where multiple physiochemical variables can play a role, remains to be seen.

3.3.3 Comparing with experiment and recommendations

The energy barriers for cellulose decomposition reported in this work are in good agreement with the modelling results presented previously in the literature [22–24,35–37], as

shown from the detailed discussion in section 3.1. The kinetic model of cellulose depolymerisation and levoglucosan formation put forward in this work can therefore be considered representative of the established cellulose pyrolysis reaction schemes (concerted mechanisms).

However, the time-dependent mass profiles presented herein, that are derived directly from well-accepted mechanisms proposed before [24–26], show clear deviations from experimental observations. In detail, the time taken for the cellulose depolymerisation process that derived from concerned mechanism is much longer than that obtained from experiment. It has been shown through experimental pyrolysis that the conversion of cellulose to LG is accomplished in under 10 seconds, even at a temperature of 500 ^{o}C, and that oligomers of cellulose larger than DP = 6 will disappear after only 3 seconds [18]. The results in this work that derived from the concerned mechanism showed that maximum conversion of cellulose to LG is not completed until around 5000 seconds at the same temperature. Furthermore, the presence of oligomers larger than DP = 16 for over 10 seconds in our kinetic analysis shows that the depolymerisation reactions are occurring much slower than is observed experimentally. This discrepancy in reaction time (or reaction rates) suggests that the four concerted depolymerisation reactions alone cannot account for the observed rates of cellulose depolymerisation and that investigation of alternative parallel depolymerisation reaction mechanisms is necessary. Additionally, the aforementioned alternative depolymerisation reactions could also account for the less than stoichiometric yields of LG. The concerted mid-chain initiation reactions considered in this work rapidly depolymerise cellulose chains to produce large numbers of smaller chains with LG-type chain-ends, from which LG is liberated through RE-depropagation reactions. As the mid-chain initiation reactions occur faster than either of the depropagation reactions, the initiation reactions are responsible for generating a significant percentage of the LG-type chain-ends. If alternative depolymerisation reactions,

that do not generate LG-type chain-ends, were reasonably competitive with the concerted initiation reactions, the number of LG-type chain ends, and therefore the yield of LG, would decrease significantly.

In a summary, the discrepancies present indication that alternative reaction pathways to the concerted mechanisms used herein must play a critical role in facilitating and limiting LG formation and require further investigation.

4. Conclusions

In this work, we have presented a kinetic model of the depolymerisation of anhydrocellulose and the formation of levoglucosan through established concerted mechanisms. At temperatures of 600 ºC and over, the breaking of large anhydrocellulose polymers proceeds rapidly, eliminating all oligomers with DP > 3 in under 10 seconds. As a result of this rapid depolymerisation, maximum LG yield is obtained after approximately 80 seconds. At 550 ºC, a maximum LG yield is not reached until around 600 seconds. It is also concluded that the time required to obtain maximum LG is independent of the initial cellulose polymer length, thus allowing for simplifications in future cellulose pyrolysis models. The kinetic results from this work agree very well with the published results from the well-accepted concerted depolymerisation reactions, however, disagree with the experimental findings, this strong indicated that alternative reaction pathways to the concerted mechanisms used herein must play a critical role in facilitating and limiting LG formation and require further investigation.

Acknowledgements

The authors would like to acknowledge financial support from the Leverhulme Trust Research Grant (RPG-2017-254) and EPSRC First Grant (EP/R010986/1). The authors are also

grateful for computational support from ARCHIE-WeSt, a regional supercomputer centre at the University of Strathclyde.

Supplementary Data

Supplementary data associated with this article was provided.

References

[1] D.F. Arseneau, Competitive Reactions in the Thermal Decomposition of Cellulose, Can. J. Chem. 49 (1971) 632–638. doi:10.1139/v71-101.

[2] I. Milosavljevic, V. Oja, E.M. Suuberg, Thermal Effects in Cellulose Pyrolysis : Relationship to Char Formation Processes, (1996) 653–662. doi:10.1021/ie950438l.

[3] C. Branca, P. Giudicianni, C. Di Blasi, GC/MS characterization of liquids generated from low-temperature pyrolysis of wood, Ind. Eng. Chem. Res. 42 (2003) 3190–3202. doi:10.1021/ie030066d.

[4] S. Thangalazhy-Gopakumar, S. Adhikari, H. Ravindran, R.B. Gupta, O. Fasina, M. Tu, S.D. Fernando, Physiochemical properties of bio-oil produced at various temperatures from pine wood using an auger reactor, Bioresour. Technol. 101 (2010) 8389–8395. doi:10.1016/j.biortech.2010.05.040.

[5] M.J.A.J. Wiliam S. -L. Mok, Effects of pressure on biomass pyrolysis. II. Heats of reaction of cellulose pyrolysis, Thermochim. Acta. 68 (1983) 165–186. doi:10.1016/0040-6031(83)80222-6.

[6] IEA Bioenergy, Country Reports: United States 2018 update, 2018.

[7] Renewable Energy Association, PHASE 1 Bioenergy in the UK-The state of play, 2019. https://www.r-e-a.net/wp-content/uploads/2019/10/REA-Bioenergy-Strategy-

425 Phase-1-State-of-Play-Web.pdf.

426 [8] H. Kawamoto, W. Hatanaka, S. Saka, Thermochemical conversion of cellulose in
427 polar solvent (sulfolane) into levoglucosan and other low molecular-weight substances,
428 J. Anal. Appl. Pyrolysis. 70 (2003) 303–313. doi:10.1016/S0165-2370(02)00160-2.

429 [9] H. Kawamoto, M. Murayama, S. Saka, Pyrolysis behavior of levoglucosan as an
430 intermediate in cellulose pyrolysis: Polymerization into polysaccharide as a key
431 reaction to carbonized product formation, J. Wood Sci. 49 (2003) 469–473.
432 doi:10.1007/s10086-002-0487-5.

433 [10] H. Kawamoto, S. Saka, Heterogeneity in cellulose pyrolysis indicated from the
434 pyrolysis in sulfolane, J. Anal. Appl. Pyrolysis. 76 (2006) 280–284.
435 doi:10.1016/j.jaap.2005.12.011.

436 [11] S. Czernik, A. V. Bridgwater, Overview of applications of biomass fast pyrolysis oil,
437 Energy and Fuels. 18 (2004) 590–598. doi:10.1021/ef034067u.

438 [12] A. Broido, M.A. Nelson, Char yield on pyrolysis of cellulose, Combust. Flame. 24
439 (1975) 263–268. doi:10.1016/0010-2180(75)90156-X.

440 [13] H. Bennadji, L. Khachatryan, S.M. Lomnicki, Kinetic Modeling of Cellulose
441 Fractional Pyrolysis, Energy and Fuels. 32 (2018) 3436–3446.
442 doi:10.1021/acs.energyfuels.7b03078.

443 [14] C.R.N. F. Shafizadeh, Y.Z. Lai, thermal degradation of 6-Chloro Carbohydrates, J.
444 Appl. Polym. Sci. 20 (1976) 139–152.

445 [15] J. Lédé, F. Blanchard, O. Boutin, Radiant flash pyrolysis of cellulose pellets: Products
446 and mechanisms involved in transient and steady state conditions, Fuel. 81 (2002)
447 1269–1279. doi:10.1016/S0016-2361(02)00039-X.

448 [16] D.K. Shen, S. Gu, The mechanism for thermal decomposition of cellulose and its main
449 products, Bioresour. Technol. 100 (2009) 6496–6504.
450 doi:10.1016/j.biortech.2009.06.095.

451 [17] P.R. Patwardhan, J.A. Satrio, R.C. Brown, B.H. Shanks, Product distribution from fast
452 pyrolysis of glucose-based carbohydrates, J. Anal. Appl. Pyrolysis. 86 (2009) 323–
453 330. doi:10.1016/j.jaap.2009.08.007.

454 [18] J.K. Lindstrom, J. Proano-Aviles, P.A. Johnston, C.A. Peterson, J.S. Stansell, R.C.
455 Brown, Competing reactions limit levoglucosan yield during fast pyrolysis of
456 cellulose, Green Chem. 21 (2019) 178–186. doi:10.1039/c8gc03461c.

457 [19] G.J. Kwon, D.Y. Kim, S. Kimura, S. Kuga, Rapid-cooling, continuous-feed pyrolyzer
458 for biomass processing. Preparation of levoglucosan from cellulose and starch, J. Anal.
459 Appl. Pyrolysis. 80 (2007) 1–5. doi:10.1016/j.jaap.2006.12.012.

460 [20] G.J. Kwon, S. Kuga, K. Hori, M. Yatagai, K. Ando, N. Hattori, Saccharification of
461 cellulose by dry pyrolysis, J. Wood Sci. 52 (2006) 461–465. doi:10.1007/s10086-005-
462 0784-x.

463 [21] G. Dobele, G. Rossinskaja, T. Dizhbite, G. Telysheva, D. Meier, O. Faix, Application
464 of catalysts for obtaining 1,6-anhydrosaccharides from cellulose and wood by fast
465 pyrolysis, J. Anal. Appl. Pyrolysis. 74 (2005) 401–405.
466 doi:10.1016/j.jaap.2004.11.031.

467 [22] X. Zhang, J. Li, W. Yang, W. Blasiak, Formation mechanism of levoglucosan and
468 formaldehyde during cellulose pyrolysis, Energy and Fuels. 25 (2011) 3739–3746.
469 doi:10.1021/ef2005139.

470 [23] X. Zhang, W. Yang, W. Blasiak, Kinetics of levoglucosan and formaldehyde

formation during cellulose pyrolysis process, Fuel. 96 (2012) 383–391. doi:10.1016/j.fuel.2012.01.006.

[24] H.B. Mayes, L.J. Broadbelt, Unraveling the reactions that unravel cellulose, J. Phys. Chem. A. 116 (2012) 7098–7106. doi:10.1021/jp300405x.

[25] X. Zhang, W. Yang, C. Dong, Levoglucosan formation mechanisms during cellulose pyrolysis, J. Anal. Appl. Pyrolysis. 104 (2013) 19–27. doi:10.1016/j.jaap.2013.09.015.

[26] R. Vinu, L.J. Broadbelt, A mechanistic model of fast pyrolysis of glucose-based carbohydrates to predict bio-oil composition, Energy Environ. Sci. 5 (2012) 9808–9826. doi:10.1039/c2ee22784c.

[27] Y. Yu, Y.W. Chua, H. Wu, Characterization of Pyrolytic Sugars in Bio-Oil Produced from Biomass Fast Pyrolysis, Energy and Fuels. 30 (2016) 4145–4149. doi:10.1021/acs.energyfuels.6b00464.

[28] J.B. Wooten, J.I. Seeman, M.R. Hajaligol, Observation and characterization of cellulose pyrolysis intermediates by 13C CPMAS NMR. A new mechanistic model, Energy and Fuels. 18 (2004) 1–15. doi:10.1021/ef0300601.

[29] M. Zhang, Z. Geng, Y. Yu, Density functional theory (DFT) study on the dehydration of cellulose, Energy and Fuels. 25 (2011) 2664–2670. doi:10.1021/ef101619e.

[30] J. Proano-Aviles, What limits the yield of levoglucosan during fast pyrolysis of cellulose?, Iowa State University, 2017. http://lib.dr.iastate.edu/etd.

[31] Y. Zhao, D.G. Truhlar, The M06 suite of density functionals for main group thermochemistry, thermochemical kinetics, noncovalent interactions, excited states, and transition elements: Two new functionals and systematic testing of four M06-class functionals and 12 other function, Theor. Chem. Acc. 120 (2008) 215–241.

494 doi:10.1007/s00214-007-0310-x.

495 [32] F. Weigend, R. Ahlrichs, Balanced basis sets of split valence, triple zeta valence and
496 quadruple zeta valence quality for H to Rn: Design and assessment of accuracy, Phys.
497 Chem. Chem. Phys. 7 (2005) 3297. doi:10.1039/b508541a.

498 [33] S. Grimme, J. Antony, S. Ehrlich, H. Krieg, A consistent and accurate ab initio
499 parametrization of density functional dispersion correction (DFT-D) for the 94
500 elements H-Pu, J. Chem. Phys. 132 (2010). doi:10.1063/1.3382344.

501 [34] M.J. Frisch, G.W. Trucks, H.B. Schlegel, G.E. Scuseria, M.A. Robb, J.R. Cheeseman,
502 G. Scalmani, V. Barone, G.A. Petersson, H. Nakatsuji, X. Li, M. Caricato, A. V.
503 Marenich, J. Bloino, B.G. Janesko, R. Gomperts, B. Mennucci, H.P. Hratchian, J. V.
504 Ortiz, A.F. Izmaylov, J.L. Sonnenberg, Williams, F. Ding, F. Lipparini, F. Egidi, J.
505 Goings, B. Peng, A. Petrone, T. Henderson, D. Ranasinghe, V.G. Zakrzewski, J. Gao,
506 N. Rega, G. Zheng, W. Liang, M. Hada, M. Ehara, K. Toyota, R. Fukuda, J.
507 Hasegawa, M. Ishida, T. Nakajima, Y. Honda, O. Kitao, H. Nakai, T. Vreven, K.
508 Throssell, J.A. Montgomery Jr., J.E. Peralta, F. Ogliaro, M.J. Bearpark, J.J. Heyd, E.N.
509 Brothers, K.N. Kudin, V.N. Staroverov, T.A. Keith, R. Kobayashi, J. Normand, K.
510 Raghavachari, A.P. Rendell, J.C. Burant, S.S. Iyengar, J. Tomasi, M. Cossi, J.M.
511 Millam, M. Klene, C. Adamo, R. Cammi, J.W. Ochterski, R.L. Martin, K. Morokuma,
512 O. Farkas, J.B. Foresman, D.J. Fox, Gaussian 16, (2016).

513 [35] Y. Zhang, C. Liu, X. Chen, Unveiling the initial pyrolytic mechanisms of cellulose by
514 DFT study, J. Anal. Appl. Pyrolysis. 113 (2015) 621–629.
515 doi:10.1016/j.jaap.2015.04.010.

516 [36] X. Zhang, W. Yang, W. Blasiak, Thermal decomposition mechanism of levoglucosan
517 during cellulose pyrolysis, J. Anal. Appl. Pyrolysis. 96 (2012) 110–119.

518 doi:10.1016/j.jaap.2012.03.012.

519 [37] S. Guo, H. Liang, D. Che, H. Liu, B. Sun, Quantitative study of the pyrolysis of
520 levoglucosan to generate small molecular gases, RSC Adv. 9 (2019) 18791–18802.
521 doi:10.1039/c9ra03138c.

522